Hyperacute Stroke: Simultaneous Measurement of Relative Cerebral Blood Volume, Relative Cerebral Blood Flow, and Mean Tissue Transit Time[1]

A. Gregory Sorensen, MD
William A. Copen, AM
Leif Østergaard, MD, MSc
Ferdinando S. Buonanno, MD
R. Gilberto Gonzalez, MD, PhD
Guy Rordorf, MD
Bruce R. Rosen, MD, PhD
Lee H. Schwamm, MD
Robert M. Weisskoff, PhD
Walter J. Koroshetz, MD

Index terms:
Blood vessels, MR, 17.12144
Brain, diffusion, 10.12144
Brain, infarction, 10.78
Brain, MR, 10.12144
Magnetic resonance (MR), diffusion study, 10.12144
Magnetic resonance (MR), vascular studies, 17.12144

Radiology 1999; 210:519–527

[1] From the Departments of Radiology (A.G.S., W.A.C., L.O., R.G.G., B.R.R., R.M.W.) and Neurology (F.S.B., G.R., L.H.S., W.J.K.), Massachusetts General Hospital, MGH-NMR Center, Bldg 149, 13th St, Charlestown, MA 02129. Received March 26, 1998; revision requested June 19; revision received July 15; accepted September 28. **Address reprint requests to** A.G.S.

Author contributions:
Guarantor of integrity of entire study, A.G.S.; study concepts, A.G.S., W.J.K., B.R.R., L.O., R.G.G.; study design, A.G.S., W.J.K., B.R.R., R.M.W., L.O., R.G.G.,; definition of intellectual content, A.G.S., W.A.C.; literature research, A.G.S., W.A.C.; clinical studies, A.G.S., W.J.K., F.S.B., L.H.S., G.R.; experimental studies, A.G.S., R.M.W.; data acquisition, A.G.S., L.H.S., G.R., F.S.B., W.J.K.; data analysis, A.G.S., W.A.C., R.M.W., L.O.; statistical analysis, A.G.S., W.A.C.; manuscript preparation and editing, A.G.S., W.A.C.; manuscript review, all authors.

PURPOSE: To investigate additional information provided by maps of relative cerebral blood flow in functional magnetic resonance (MR) imaging of human hyperacute cerebral ischemic stroke.

MATERIALS AND METHODS: Diffusion-weighted and hemodynamic MR imaging were performed in 23 patients less than 12 hours after the onset of symptoms. Maps of relative cerebral blood flow and tracer mean tissue transit time were computed, as were maps of apparent diffusion and relative cerebral blood volume. Acute lesion volumes on the maps were compared with follow-up imaging findings.

RESULTS: In 15 of 23 subjects (65%), blood flow maps revealed hemodynamic abnormalities not visible on blood volume maps. A mismatch between initial blood flow and diffusion findings predicted growth of infarct more often (12 of 15 subjects with infarcts that grew) than did a mismatch between initial blood volume and diffusion findings (eight of 15). However, lesion volumes on blood volume and diffusion maps correlated better with eventual infarct volumes ($r > 0.90$) than did those on blood flow and tracer mean transit time maps ($r \sim 0.6$), likely as a result of threshold effects. In eight patients, blood volume was elevated around the diffusion abnormality, suggesting a compensatory hemodynamic response.

CONCLUSION: MR imaging can delineate areas of altered blood flow, blood volume, and water mobility in hyperacute human stroke. Predictive models of tissue outcome may benefit by including computation of both relative cerebral blood flow and blood volume.

Stroke remains the third leading cause of death and the major cause of adult disability in the United States. Intravenously administered recombinant tissue-type plasminogen activator (rtPA, alteplase; Genentech, South San Francisco, Calif) has been approved by the U.S. Food and Drug Administration for treatment of hyperacute cerebral ischemia in the first 3 hours after the onset of symptoms. Findings in studies of intravenous thrombolytic therapy that allowed later administration demonstrated increased likelihood of death, likely due to intracranial hemorrhage (1,2). Hemorrhage rates may be especially high in patients with abnormal CT scans before administration of intravenous thrombolytics (3). In contrast, data from human positron emission tomography (PET) and magnetic resonance (MR) imaging studies indicate that the therapeutic window for salvaging some brain tissue by means of reperfusion may be wider than 3 hours (4–6). A diagnostic tool that could assess the presence or absence of salvageable brain tissue, as well as the risk of hemorrhage into injured tissue, might allow therapy to be tailored for individual subjects.

Recent advances in the availability and capability of MR imaging may provide such a

tool. Methods have been described that allow MR imaging to provide images or maps of relative cerebral blood flow and the mean transit time of a tracer through the tissue. This is in addition to the relative cerebral blood volume and the diffusion-weighted images already in use in some centers. More accurate markers could then be used to assess the risks and benefits of therapeutic interventions. We hypothesize that the additional information provided by images of relative cerebral blood flow and tracer mean transit time might better characterize acute cerebral infarction than information from relative cerebral blood volume maps and diffusion-weighted images alone. In this study, we compared lesion volumes on initial and follow-up MR images in subjects after hyperacute stroke. We sought to determine whether mismatches between blood flow and blood volume exist in human hyperacute stroke. We also sought to determine if mismatches between blood flow and diffusion lesions predicted lesion growth.

TABLE 1
Patient Demographic Data

Patient/ Age (y)/Sex	Presenting Symptom	Time after Presentation to MR Imaging: Initial (h)	Time after Presentation to MR Imaging: Follow-up (d)
1/35/M	Left hemiparesis	7.0	5
2/68/M	Left hemiparesis	10.0	6*
3/62/M	Right hemiparesis and aphasia	7.0	14
4/72/F	Left hemiparesis	2.5	5
5/55/M	Right hemiparesis	2.0	3
6/85/F	Left hemiparesis	5.5	7
7/60/M	Left hemiparesis	3.0	11
8/53/M	Left hemiparesis and hemineglect	3.0	3*
9/91/F	Left hemiparesis	5.0	5*
10/50/M	Left hemiparesis	4.5	6*
11/62/F	Left hemiparesis	7.5	17
12/79/M	Left facial weakness	7.0	4
13/66/M	Right hemiplegia and Broca aphasia	2.5	3
14/58/M	Dysarthria and right facial weakness	6.0	5
15/72/M	Aphasia	6.0	54
16/48/F	Right hemiparesis and aphasia	1.5	7
17/69/M	Right inferior quadrantanopia and left-sided numbness	10.0	277
18/64/F	Left arm and leg weakness	5.5	7
19/78/F	Aphasia	4.0	5
20/42/F	Right hemiplegia	10.0	59
21/75/M	Mutism	4.0	4*
22/79/M	Ataxia and vertigo	6.5	7
23/33/M	Right hemiplegia and mutism	4.0	17

* Follow-up imaging used for volume calculation was CT rather than MR imaging.

MATERIALS AND METHODS

All imaging protocols were approved by our institutional subcommittee on human studies. For patients included in this study, written informed consent was obtained from the patient or family before MR imaging.

Patient Selection

Patients presenting with acute hemiparesis, hemiplegia, or aphasia were evaluated by our service as described previously (7). Evaluation included x-ray computed tomography (CT) of the head. For this study, patients were enrolled consecutively. Potential subjects were excluded if the last time they were witnessed to be without symptoms was greater than 12 hours earlier, if no intravenous access could be obtained, if the patient's condition was deemed too unstable to allow MR imaging, or if the patient was enrolled in a clinical trial of a stroke therapy agent. Patients were excluded if complete or follow-up studies were not available. No patients in this study received tissue plasminogen activator or intraarterial thrombolytics.

Each patient was subsequently treated as deemed appropriate. We also included in this study the nine patients from our first study (7) who had a diffusion abnormality on their initial imaging study.

Conventional MR Imaging

MR imaging was performed with a 1.5-T MR imaging unit (Signa; GE Medical Systems, Milwaukee, Wis) with an echo-planar retrofit (Advanced NMR Systems, Wilmington, Mass). We made two modifications to the hyperacute stroke MR protocol we used earlier (7). In this study, diffusion-weighted imaging included measurement of the full diffusion tensor, and postprocessing included maps of relative cerebral blood flow and tracer mean tissue transit time. These changes did not alter the time required for the examination; when combined with two-dimensional phase-contrast MR angiography, our entire protocol required approximately 30 minutes (about 15 minutes of imaging time). Follow-up CT or MR imaging studies were performed between 3 and 59 days (median, 6 days).

Diffusion-weighted MR Imaging

With our earlier technique, three orthogonal components of the diffusion tensor were sampled, and the trace and an isotropic diffusion-weighted image were computed (7). In this study, we modified this technique to sample the entire diffusion tensor. This consists of acquisition of six high-*b*-value, single-shot images at each section, each corresponding to diffusion measurement in a given direction, followed by acquisition of a single low-*b*-value image. The high *b* value was 1,221 sec/mm^2, and the low *b* value was 3 sec/mm^2. Imaging parameters included the following: repetition time, 6 seconds; echo time, 118 msec; matrix, 256 $\times$ 128; field of view, 40 $\times$ 20 cm; section thickness, 6 mm; and intersection gap, 1 mm. The complete seven-image tensor acquisition required 42 seconds; we typically acquired three repetitions to improve the signal-to-noise ratio, which resulted in a total imaging time of 126 seconds. Generation of isotropic (tensor trace) diffusion-weighted images occurred off-line on a network workstation (Sparcstation 20; Sun Microsystems, Milpitas, Calif) and required 5–10 minutes for data transfer and computation.

Hemodynamic Imaging

Hemodynamic imaging was performed with gradient-echo or spin-echo echo-planar techniques during the injection of 0.1 (gradient-echo) or 0.2 (spin-echo) mmol per kilogram of body weight gadodiamide (Omniscan; Nycomed, Oslo, Norway) or gadopentetate dimeglumine (Magnevist; Berlex Laboratories, Wayne,

TABLE 2
Lesion Volume (in cubic centimeters) on Images

Patient No.	Diffusion-weighted	Cerebral Blood Volume	Cerebral Blood Flow	Mean Tissue Transit Time	Follow-up
1	2.5	2.5	2.4	0.5	2.7
2	8.5	28.5*	161.7*	162.5*	18.2*
3	24.5	63.4*	107.6*	117.9*	119.1*
4	9.6	8.2	174.3*	175.3*	18.2*
5	6.2	49.6*	270.4*	257.0*	19.5*
6	13.6	43.1*	168.4*	157.1*	19.1*
7	5.2	1.5	0.9	0.0	0.8
8	174.7	196.5	228.7*	191.9	211.0*
9	200.4	208.5	214.4	312.2*	282.7*
10	30.1	83.5*	216.5*	219.4*	179.7*
11	30.1	24.9	51.0*	32.1	33.8
12	15.6	5.1	4.9	2.6	14.7
13	25.5	10.8	13.5	0.7	105.6*
14	4.4	1.2	0.0	1.2	4.3
15	38.3	20.8	41.3	42.9	12.3
16	7.2	3.5	4.4	2.9	17.0*
17	8.0	1.9	1.9	0.0	1.5
18	1.5	0.0	16.1*	44.5*	2.5*
19	20.8	21.6	75.2*	84.0*	87.0*
20	1.6	1.0	1.8	0.8	1.5
21	12.0	14.8*	15.7*	20.3*	15.5*
22	7.1	12.1*	23.8*	33.1*	14.3*
23	30.8	100.7*	342.5*	431.2*	105.3*

* Measurement is more than 15% larger than the initial abnormality depicted on diffusion-weighted images.

NJ). This dynamic susceptibility contrast imaging technique produces images from which a variety of synthetic maps can be synthesized (8–11) and typically produced a maximum signal intensity drop of 20%–30% on spin-echo echo-planar images. We obtained either 51 single-shot echo-planar images in each of 10 sections, for a total of 510 complete images acquired in 83 seconds, or 46 single-shot echo-planar images in each of 11 sections, for a total of 506 complete images acquired in 69 seconds. Data were transferred to workstations for further analysis.

To determine cerebral blood flow, we used the following expression to describe the concentration of intravascular contrast agent within a given volume of interest (C_{VOI}) as a function of time (t):

$$C_{VOI}(t) = F_t \int_0^t C_a(\tau)R(t-\tau)d\tau, \quad (1)$$

where F_t is tissue flow, C_a is the arterial input function, and $R(t)$ is the vascular *residue function*, describing the fraction of tracer still present in the vascular bed of the volume of interest at time t after injection of a unit impulse of tracer in its feeding vessel. Equation (1) is the central equation in any approach to determine flow by using nondiffusible tracers, as it states that the initial height of the deconvolved concentration time curve equals the flow, F_t. However, Equation (1) is not straightforward to solve for F_t because $R(t)$ is an unknown function dependent on local vascular structure.

Determination of cerebral blood flow from intravascular tracers is a complex task. Approaches to solve Equation (1) can be classified into two groups. In a model-dependent approach, an empiric analytic expression is chosen to describe vascular retention (that is, $R[t]$) of contrast agent. In a model-independent approach, cerebral blood flow and the vascular retention of tracer are determined by means of nonparametric deconvolution.

We determined by means of simulations that traditional model-dependent analytic expressions can yield absolute flow if the actual underlying residue function was sufficiently described by the applied model. Findings in our simulations indicated that this approach still may yield reasonable relative flow values if the shape of the residue function is relatively uniform across the brain even if the assumed model is not well matched by the true residue function. However, in the presence of pathologic and altered hemodynamics, when the shape of the residue function may vary spatially, use of this approach may lead to statistically significant errors in measurements of relative flow.

To address this difficulty, we developed a model-independent approach. In this approach, nonparametric deconvolution is performed to determine $R(t)$ and F_t simultaneously in Equation (1). We investigated several approaches for performing nonparametric deconvolution. Approaches we evaluated were required to be capable of determining absolute and relative flow with good accuracy, independent of the underlying vascular structure and volume (12), and with raw image signal-to-noise ratios equivalent to those obtainable with current clinical protocols (13). The deconvolution approach we found most useful is singular value decomposition.

Our technique depends on deconvolution with an arterial input function. Voxels that compose this arterial input function are manually selected by choosing voxels near the middle cerebral artery that supplies the unaffected hemisphere. For each voxel, the time-intensity curve for the dynamic images is converted first to a curve of change in T2, or $\Delta R2$, and then of concentration versus time. Relative cerebral blood volume (CBV) is then computed by means of a numeric integration technique as described previously (14–16). From our flow and volume maps, maps of true mean transit time (MTT) of the tracer can be computed by means of the relationship specified by the central volume theorem: $MTT = CBV/F_t$.

Lesion Volume Measurement

To measure the volume, we used a simple planimetric technique that is similar to other approaches (7,17). The various images were transferred to a personal computer (Macintosh; Apple Computer, Cupertino, Calif), where the abnormality was outlined by using a commercially available software package (ALICE; Hayden Image Processing Solutions, Boulder, Colo). This software package has a segmentation tool that suggests an initial contour on the basis of local image intensity gradients. This contour was then modified to exclude nonanatomic regions (eg, choroid plexus) by a research assistant (W.A.C.), and the contour was edited or confirmed by a neuroradiologist (A.G.S.) by using all the available images. Lesion volume was then calculated by multiplying the number of voxels by the volume of a single voxel. The follow-up infarct volume was determined by calculating the lesion volume on the last imaging study available (either CT or MR imaging) in a similar manner. (We used CT as the final study only when MR images were not available; in our experience, these two volumes are generally quite similar). We chose this planimetric

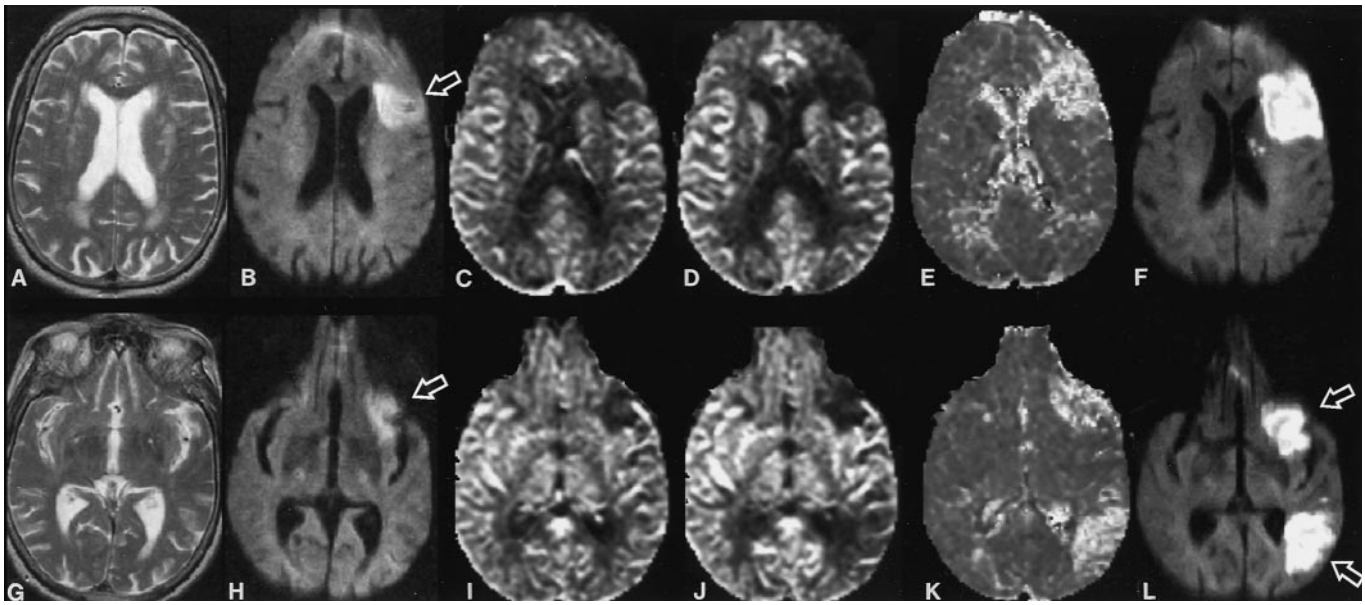

Figure 1. Patient 19. Sensitivity of relative cerebral blood flow and tracer mean transit time to ischemia. *A–E* and *G–K* were obtained 3 hours after the onset of aphasia that occurred during cardiac catheterization. *A–F*, Upper anatomic section. *A*, T2-weighted image is normal. *B*, Diffusion-weighted image demonstrates hyperintensity in the left frontal lobe (arrow) consistent with the patient's symptoms. Hemodynamic images including relative cerebral blood volume (*C*), relative cerebral blood flow (*D*), and tracer mean transit time (*E*) depict a similar, slightly larger abnormality. *F*, Follow-up diffusion-weighted image obtained at 5 days depicts infarction. *G–L*, Lower anatomic section. *G*, T2-weighted image again shows no abnormality. *H*, Diffusion-weighted image depicts an inferior frontal lobe hyperintensity (arrow) consistent with ischemia. Hemodynamic images show no apparent change in relative cerebral blood volume (*I*), but a 75% drop in relative cerebral blood flow (*J*), and a doubling of tracer mean transit time (*K*). *L*, Follow-up diffusion-weighted image also obtained at 5 days depicts a second area of infarct as well as the first (arrows).

method rather than a numeric threshold method because our earlier results demonstrated that MR imaging–based techniques are sensitive enough to depict the roughly two-to-one physiologic gray-white differences in relative cerebral blood flow and relative cerebral blood volume. These gray-white differences would interfere with simple threshold-based volume calculations, particularly in lesions that involve both gray and white matter (the majority of lesions). We also used this semiautomated technique rather than a threshold-based technique because it more nearly simulated how these maps might be used in clinical practice—that is, the area thought to be visually abnormal by an interpreter who does not know the eventual outcome.

When comparisons were made for possible mismatch between initial and follow-up findings for diffusion-weighted images, relative cerebral blood flow, relative cerebral blood volume, or tracer mean transit time, up to 15% change was allowed before a difference was considered meaningful. (For example, the lesion on the blood flow map had to be greater than 1.15 times the volume of the lesion on the diffusion-weighted image.) This was to account for effects of volume averaging and possible head position changes.

Region-of-Interest Analysis

In each patient, three regions of interest were placed manually: (*a*) in the center of the cerebral blood volume abnormality, (*b*) in an area of mismatch between the maps of cerebral blood flow and cerebral blood volume (high signal intensity on the mean transit time images), and (*c*) in the center of the diffusion-weighted imaging abnormality. The regions of interest were defined as 9-voxel collections in a single section (typically 3×3 voxels). Voxels with signal intensity insufficient to allow valid determination of results were avoided.

Statistical Analysis

Lesion volume measurements on the initial study were correlated with those on the follow-up study by means of a Spearman rank correlation coefficient. Then, for each of the four primary functional MR imaging maps (diffusion-weighted image, relative cerebral blood flow, relative cerebral blood volume, and tracer mean transit time), if there was a statistically significant correlation between the initial and follow-up lesion volume, the two volumes were plotted, and a linear fit was performed (constrained by a forced zero intercept).

In addition, region-of-interest mean signal intensities from the regions of interest located in the centers of the cerebral blood volume abnormality were compared with the mean signal intensities from the regions of interest located in the area of mismatch between the lesion on diffusion-weighted images and the lesion on blood flow maps. Comparison was made with a Wilcoxon signed rank test of the paired values on a patient-by-patient basis.

RESULTS

The overall CT, conventional MR imaging, diffusion-weighted imaging, hemodynamic imaging, and follow-up results are summarized in Tables 1 and 2. In all patients, the diagnosis of hyperacute cerebral ischemia was confirmed at follow-up imaging. Figure 1 shows images of tracer mean transit time and relative cerebral blood flow abnormalities that depicted a second, distant focus of abnormal blood flow that proceeded to infarction. Figure 2 shows images of such abnormalities that did not proceed to infarction. Figure 3 shows images that depict probable spontaneous reperfusion.

In 20 of the 23 patients, lesion volume

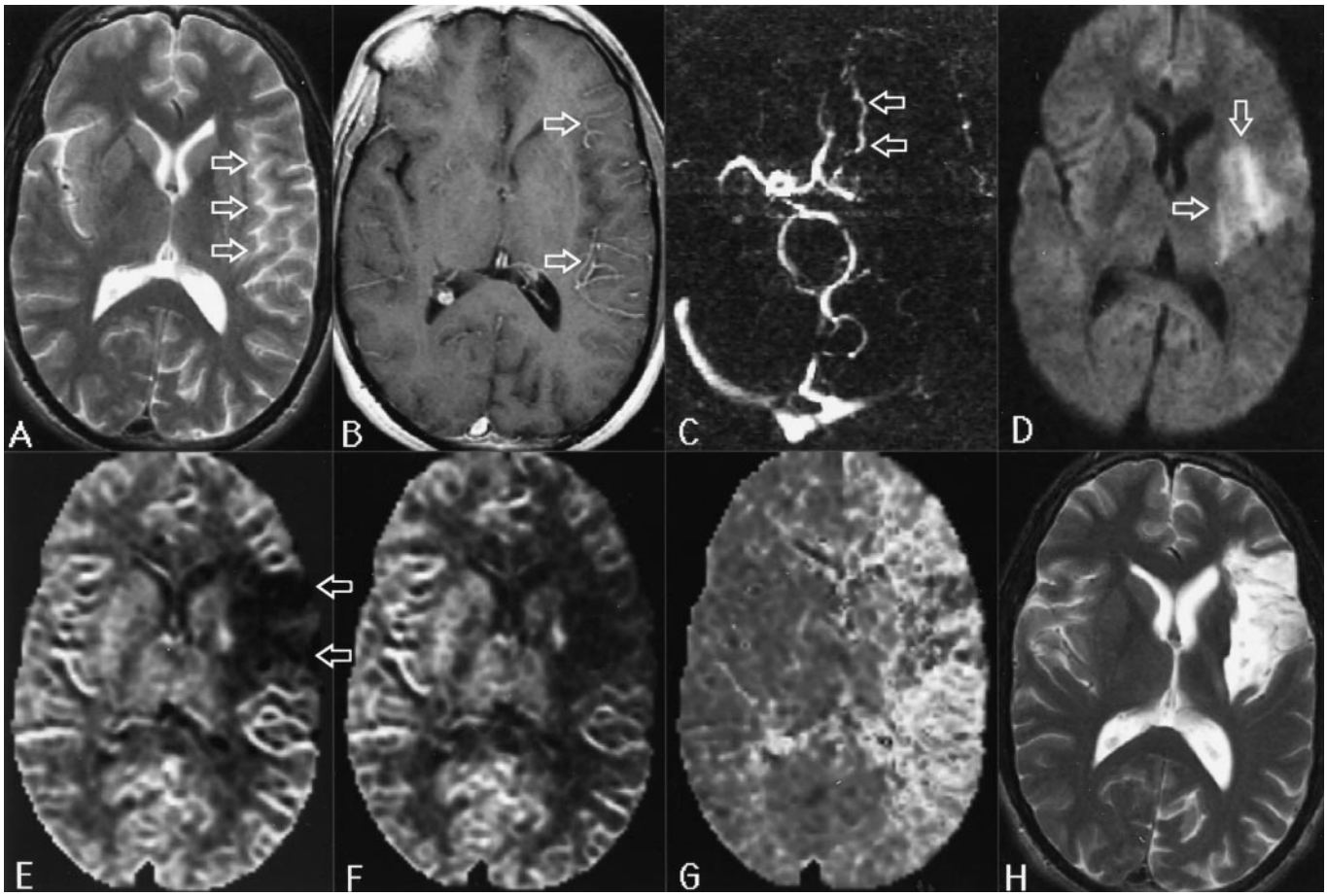

Figure 2. Patient 23. Specificity for ischemia of relative cerebral blood volume, relative cerebral blood flow, and tracer mean transit time. *A–G* were obtained 4 hours after the onset of right-sided hemiplegia and mutism. *A*, T2-weighted image shows sulcal effacement (arrows). *B*, Contrast material–enhanced T1-weighted image demonstrates contrast in multiple dilated vessels (arrows) in the affected hemisphere, consistent with slow flow. *C*, Phase contrast MR angiogram demonstrates absence of flow in the left internal carotid and middle cerebral arteries. Note the prominent ophthalmic artery (arrows), which directional MR angiography (not shown) depicted as having retrograde flow. *D*, Diffusion-weighted image demonstrates hyperintensity (arrows) in the left hemisphere consistent with the patient's symptoms. Hemodynamic images including relative cerebral blood volume (*E*), relative cerebral blood flow (*F*), and tracer mean transit time (*G*) depict a larger area of decrease (arrows in *E*) in *F* than in *E* or *G*, consistent with occlusion of the middle cerebral artery branch but collateral flow. *H*, Follow-up T2-weighted image obtained at 7 months depicts the infarction as smaller than the flow abnormality in *F* but larger than the diffusion abnormality in *D*.

on the follow-up diffusion-weighted image was greater than or equal to that on the initial image. Among the three remaining patients, the initial and follow-up lesion volumes were too small to allow any definite conclusions in one, and the follow-up lesion volume was clearly smaller than the initial lesion volume in two. In one of the latter patients (patient 17), initial relative cerebral blood flow and relative cerebral blood volume had increased rather than decreased in the area of abnormality on the diffusion-weighted images, suggesting early spontaneous reperfusion.

Among the 23 patients, the follow-up lesion volume was smaller than the initial lesion volume on relative cerebral blood flow images in 17. The follow-up volume was more than 15% larger than the initial volume on diffusion-weighted images in 15. A mismatch existed between the lesion volume on the initial diffusion-weighted images and on the maps of relative cerebral blood volume in eight, all of whom had infarct growth. A mismatch existed between the lesion volume on the initial diffusion-weighted images and on the maps of relative cerebral blood flow in 13, 12 of whom had infarct growth. A mismatch existed between the lesion volume on the initial diffusion-weighted images and on the maps of tracer mean transit time in 12, all of whom had infarct growth.

Analysis of Spearman rank correlation coefficients demonstrated high (and statistically significant) correlation between follow-up infarct volume and lesion volume on initial diffusion-weighted images, maps of relative cerebral blood flow, relative cerebral blood volume, and tracer mean transit time (Table 3). In Figure 4, the relationships between the initial lesion volumes and follow-up infarct volumes are plotted. As we reported earlier in a smaller group of patients (7), these scatterplots depict that follow-up infarct volume is almost always underestimated on initial diffusion-weighted images and relative cerebral blood volume maps. In this group of patients, however, infarct volume was almost always overestimated—as visually defined—on initial maps of relative cerebral blood flow and tracer mean transit time.

Table 4 lists the region-of-interest measurements. In the core of the abnormality, the mean apparent diffusion coefficient was 46% of that in the contralateral hemisphere, and mean relative cerebral blood volume, relative cerebral blood

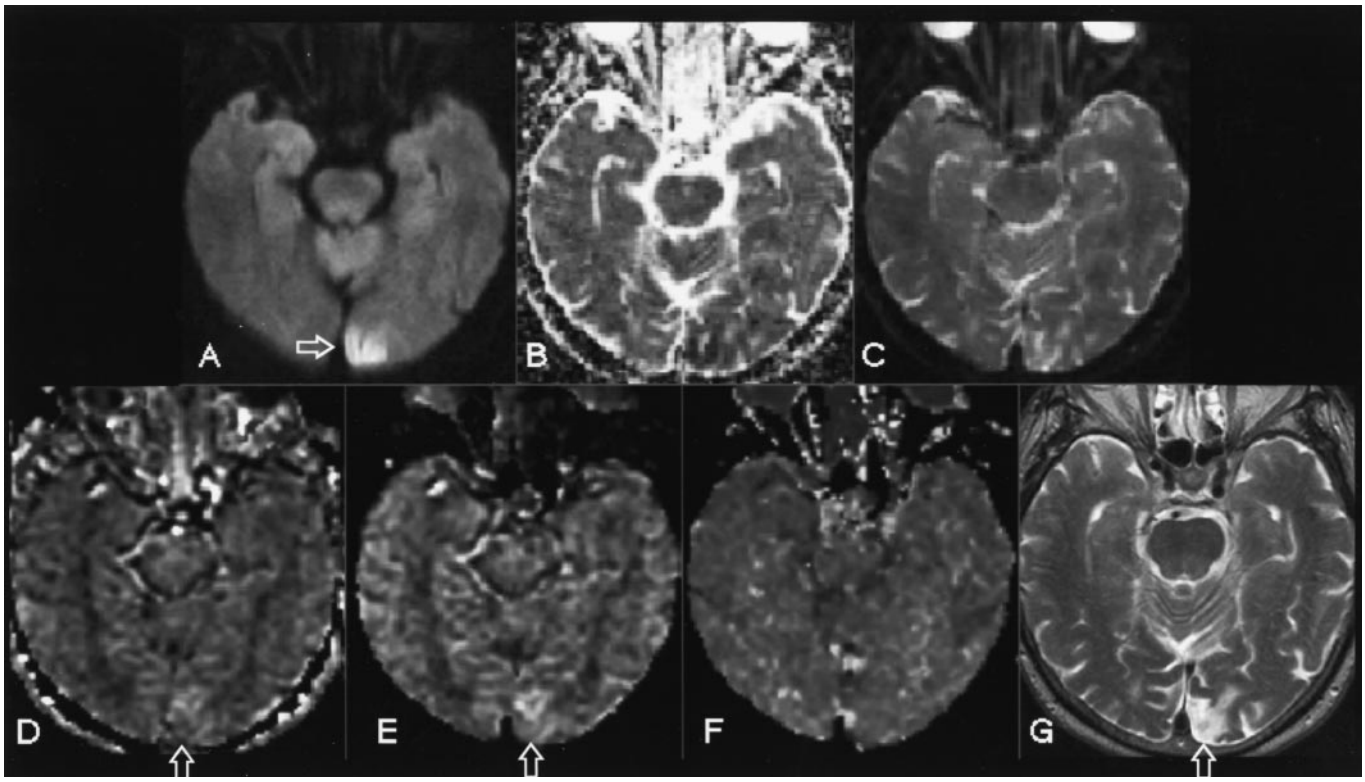

Figure 3. Patient 17. Spontaneous reperfusion. *A–F* were obtained 10 hours after the onset of a right-sided quadrantanopia and left-sided numbness. Diffusion-weighted image (*A*) and trace apparent diffusion coefficient map (*B*) depict abnormal water mobility in the left occipital lobe (arrow in *A*). *C*, Echo-planar T2-weighted image was also subtly abnormal (conventional T2-weighted images [not shown] were degraded by motion artifact). Hemodynamic images including relative cerebral blood volume (*D*), relative cerebral blood flow (*E*), and tracer mean transit time (*F*) depict increased blood flow and blood volume (arrow) in the area of diffusion abnormality, suggesting spontaneous reperfusion prior to initial imaging. *G*, Follow-up image obtained at 9 months shows infarction (arrow) with focal low relative cerebral blood volume (not shown). The ability to document such spontaneous reperfusion may help identify patients no longer in need of chemical or mechanical thrombolysis. Such patients can thereby avoid the risks associated with thrombolytic therapy.

flow, and mean transit time were, respectively, 9%, 26%, and 211% of those in the contralateral hemisphere. Spearman rank analysis was performed to determine any correlation between the apparent diffusion coefficient, relative cerebral blood flow, relative cerebral blood volume, or tracer mean transit time in the core of the lesion, or between the time from onset of symptoms to imaging and any of these values. A high correlation was demonstrated between only relative cerebral blood volume and relative cerebral blood flow ($P < .001$).

Table 4 also demonstrates that mean relative cerebral blood flow and mean relative cerebral blood volume are lower, and tracer mean transit time is higher, in the core than in the periphery, as might be expected. However, in eight patients, the initial relative cerebral blood volume was above 1.0 in the periphery, suggesting an increase in local capillary volume. The mean relative cerebral blood volume and mean relative cerebral blood flow in the periphery were higher in these eight patients than in the 15 other patients.

TABLE 3
Correlation Values between Lesion Volumes

Type of Image or Map	Cerebral Blood Volume	Cerebral Blood Flow	Tracer Mean Transit Time	Follow-up
Diffusion-weighted	0.9212	0.4394*	0.4683†	0.8535
Cerebral blood volume		0.7106	0.7274	0.9047
Cerebral blood flow			0.9726	0.5705
Tracer mean transit time				0.6050

Note.—$P = .0001$ (Spearman rank correlation coefficient).
* $P = .002$.
† $P = .01$.

DISCUSSION

Our results confirm those of earlier reports that with functional MR imaging cerebral ischemia can be sensitively detected and to some degree characterized (18–20). Our results also suggest that initial diffusion-weighted images underestimate follow-up infarct volume in untreated patients (6,21). Our data also confirm the mismatch between blood volume and blood flow depicted with PET and indicate that this mismatch can be measured with MR imaging. Our data extend previous results by demonstrating that (*a*) relative cerebral blood flow can be measured routinely with MR imaging; (*b*) the cerebral hemodynamic abnormalities associated with hyperacute cerebral ischemia include changes in both blood volume and blood flow; and (*c*) measurement of relative cerebral blood flow may

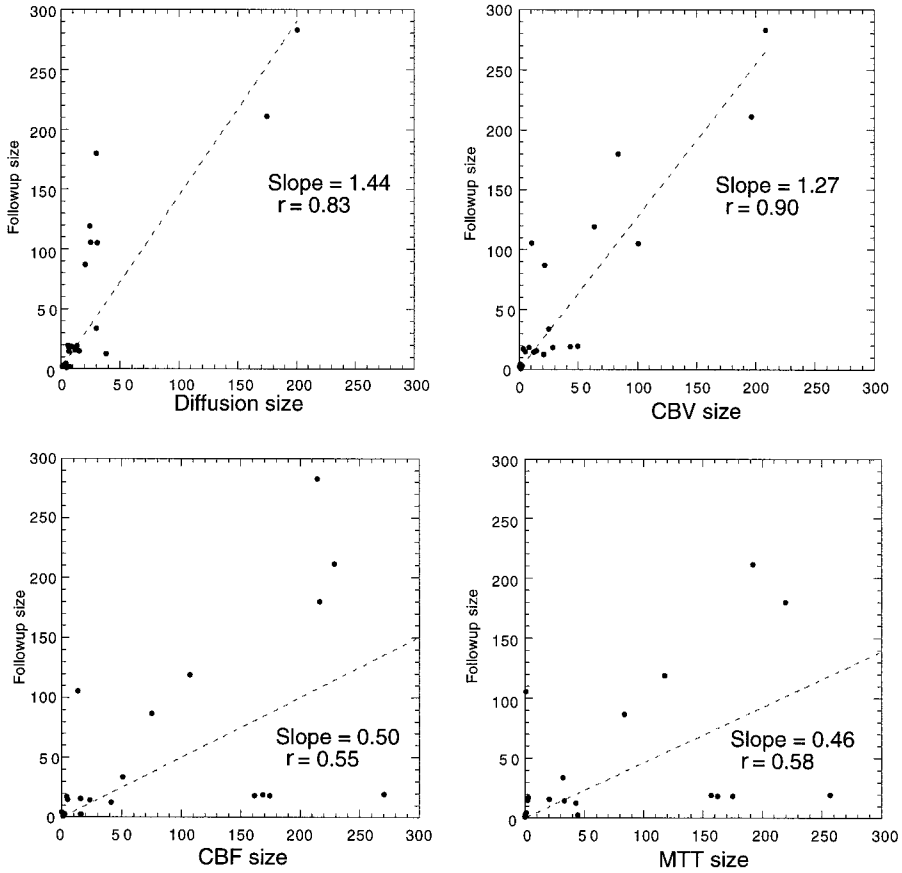

Figure 4. Scatterplots of initial versus follow-up lesion volume demonstrate that cerebral blood volume (*CBV*) has the highest correlation (*r*) to a linear fit and the slope closest to 1.0. *CBF* = cerebral blood flow, *Diffusion* = diffision-weighted image, *MTT* = mean transit time.

be more powerful when combined with other measurements, such as diffusion-weighted imaging, rather than when used alone.

Figures 1–3 depict how the addition of perfusion information can rationalize the interpretation of the diffusion-weighted imaging findings. In Figure 1, the tracer mean transit time abnormality clearly points out an area at risk that had only 25% of normal relative cerebral blood flow and proceeded to infarction. In Figure 2, the tracer mean transit time is abnormal, but the cerebral blood volume depicts collateral flow, and the cerebral blood flow abnormality is only mild. Figure 3 shows increased initial relative cerebral blood volume and blood flow, which suggests spontaneous reperfusion of the once ischemic focus. This range of findings supports the variability of cerebral ischemia in humans. Assessment of such variability will likely be useful in tailoring thrombolytic and other therapies for specific patients. For example, one testable hypothesis suggested by these data is that thrombolytic therapy does not offer any benefit in patients with completely matched abnormalities on diffusion-weighted images and cerebral blood flow maps obtained at presentation.

This variability in initial insult is also seen by comparing initial and follow-up lesion volumes: No one predictor is sufficient to determine infarct size, not even relative cerebral blood flow. When a mismatch (between the lesion volume on initial blood flow maps and initial diffusion-weighted images) was observed, the infarct enlarged on the follow-up images in 12 of 13 patients, but the degree of future infarction was not accurately predicted by using our visual planimetric approach. Rather, it is likely that the combination of relative cerebral blood flow, relative cerebral blood volume, tracer mean transit time, apparent diffusion coefficient, and T2 (and perhaps other markers) into an appropriate tissue characterization model will allow distinction of tissue that is definitely infarcted, that is at high risk for future infarction, and that is at low risk. We speculate that part of this variability between initial and follow-up findings is due to the inconsistent duration and sequence of pathophysiologic events that can occur after initial ischemia as a result of differences in both local and systemic vascular physiology (22). It seems unlikely that imaging findings at 6 hours will be able to predict some types of future changes such as spontaneous reperfusion, migration of the embolus distally, or systemic hypotension. As a result, the role of MR imaging may be to indicate what is likely in the immediate rather than distant future.

Such variability in lesion volume on initial and follow-up relative cerebral blood flow maps also indicates that any measurement of cerebral blood flow alone—with MR imaging, PET, or xenon-enhanced CT—may not be as helpful as the coupling of measurements of relative cerebral blood flow with markers of the tissue response to the low cerebral blood flow. In effect, such metabolic markers might help integrate the severity of the decrease in relative cerebral blood flow and its duration. Diffusion-weighted imaging, though still incompletely understood, provides a rapid and simple map of metabolic state, possibly including changes due to severe adenosine triphosphate depletion in the brain. PET could also provide such information with oxygen extraction or other metabolic markers.

Our data indicate that MR imaging can elucidate some of the early pathophysiologic events in cerebral ischemia. The elevation of relative cerebral blood volume around the ischemic (abnormal diffusion) zone is consistent with findings in animal studies that show a compensatory vasodilation in reduced perfusion pressure in an attempt to maintain oxygen delivery. We speculate that vasodilation of leptomeningeal collateral vessels may delay additional cortical damage in patients with injury in the poorly collateralized basal ganglia regions.

The low correlation between lesion volume on initial and follow-up maps of relative cerebral blood flow or tracer mean transit time might be due to our manual segmentation approach. It is possible that predictive capability might improve when improved segmentation approaches are applied to a single physiologic parameter such as relative cerebral blood flow. Relative cerebral blood volume and blood flow images demonstrate the expected gray-white ratios, as documented in our earlier work (13), and therefore can obscure subtle findings, particularly those at the gray-white junctions. Given such gray-white differences, a single value of rela-

TABLE 4
Core and Peripheral Mean Region-of-Interest Values, Relative to Contralateral Hemisphere

	Core				Peripheral		
Patient No.	Apparent Diffusion Coefficient	Relative Cerebral Blood Volume	Relative Cerebral Blood Flow	Tracer Mean Transit Time	Relative Cerebral Blood Volume	Relative Cerebral Blood Flow	Tracer Mean Transit Time
1	0.67	0.42	0.21	2.50	0.35	0.13	3.02
2	0.33	0.59	0.44	1.39	0.42	0.06	9.16
3*	0.05	0.18	0.09	2.19	1.09	0.58	1.90
4*	0.56	0.16	0.18	0.88	1.20	0.55	2.31
5	0.31	0.44	0.38	1.21	0.83	0.34	2.49
6*	0.47	0.08	0.06	1.54	5.17	2.48	2.07
7	0.60	0.44	0.26	2.78	0.75	0.40	1.90
8	0.44	0.13	0.06	2.81	0.60	0.30	1.98
9	0.45	0.07	0.08	0.87	0.51	0.17	2.97
10	0.52	0.27	0.11	2.45	0.90	0.28	3.21
11	0.18	0.21	0.10	2.30	0.82	0.29	2.86
12	0.35	0.12	0.08	1.71	0.25	0.13	2.14
13	0.48	0.32	0.42	0.73	0.34	0.18	1.98
14*	0.78	0.30	0.50	0.61	5.37	2.23	2.38
15	0.36	0.35	0.43	0.98	0.81	0.46	1.75
16	0.51	0.16	0.14	1.15	0.61	0.31	1.95
17*	0.37	1.43	1.33	1.13	1.71	1.47	1.18
18*	0.63	0.82	0.36	2.28	2.19	0.77	2.80
19	0.37	0.10	0.08	1.30	0.86	0.38	2.30
20	0.63	0.40	0.31	1.53	0.45	0.20	2.11
21*	0.58	0.12	0.15	0.85	1.03	0.59	1.73
22	0.32	0.23	0.31	0.78	0.71	0.38	1.90
23*	0.50	0.24	0.15	1.67	1.45	0.44	3.33
Mean	0.45	0.33	0.27	1.55	1.24	0.57	2.58
SD	0.16	0.30	0.27	0.70	1.35	0.63	1.53
Mean*	0.49	0.42	0.35	1.39	2.40	1.14	2.21
SD*	0.22	0.47	0.42	0.63	1.81	0.82	0.66

Note.—Lesions localized on diffusion-weighted images; regions of interest may not be placed identically on core images because coregistration was not performed. However, each triplet of hemodynamic variable values comes from the same region of interest, either core or periphery.

* Includes only those subjects with peripheral relative cerebral blood volume ≥ 1.0. Differences in mean peripheral relative cerebral blood volume and relative cerebral blood flow, $P < .001$.

tive cerebral blood flow is unlikely to be a suitable threshold for both gray and white matter ischemia. The planimetric technique used in this study is less than ideal, but it is useful in the face of such differences.

Tracer mean transit time images are straightforward to interpret visually because of the lack of gray-white differences in normal brain (which is evidence of the normal coupling of relative cerebral blood flow and blood volume). In our day-to-day practice, we have found that the maps of tracer mean transit time are highly sensitive to this flow-volume uncoupling; however, if they depict an abnormality, it must be confirmed as in an ischemic range on the maps of relative cerebral blood flow before it can be considered a marker of ischemia rather than of oligemia.

Finally, our results are useful in the ongoing effort to better model relative cerebral blood flow with MR imaging. There are theoretic reasons why measurement of relative cerebral blood flow with an intravascular tracer is challenging. In particular, we were interested in determining whether the mathematic assumptions in our approach about the relationship between flow and volume in normal brain would preclude assessment of abnormal brain. Also, note that the tracer mean transit time we report here is derived from measurements of flow, not from the width of the bolus. Use of non–flow estimates of mean transit time may lead to inaccuracies (23).

Our technique has some limitations, but it appears to be suitable for imaging of hyperacute stroke. One such limitation is that all intravascular tracer methods require delivery of the tracer to allow measurements, and therefore relative cerebral blood volume may in fact be much larger than that measured with our approach simply because no tracer is reaching dilated but nonperfused blood vessels. However, if tracer cannot reach a portion of brain tissue, it is unlikely that freshly oxygenated blood could reach this same tissue. Furthermore, this shortcoming would only obscure the flow-volume mismatch, and our images document that we are still able to identify flow-volume mismatches with regularity. Another limitation with our technique is that delays in arrival of contrast material may be interpreted as decreases in flow, and therefore collateral flow may not be adequately represented. More mathematic work is needed to further improve this technique for ongoing use in the evaluation of human hyperacute cerebral ischemia. We also plan validation of findings with this technique by comparing our approach with other technologies such as PET.

In conclusion, measurement of relative cerebral blood flow with MR imaging is possible in patients after hyperacute stroke and provides additional diagnostic information. Relative cerebral blood flow and tracer mean transit time imaging are as feasible in the same routine clinical setting as are diffusion-weighted and relative cerebral blood volume imaging, and the findings appear to be useful predictive indicators when used in concert with

other functional MR imaging findings. The mismatch between abnormalities in apparent diffusion coefficient (which indicate metabolically injured brain) and hemodynamic abnormalities (which indicate abnormal tissue perfusion) can be visualized. With further study, these tools may be able to yield information about the time-dependent probability of a specific therapy being able to limit infarct size in individual patients after ischemic stroke.

References

1. Anonymous. Thrombolytic therapy with streptokinase in acute ischemic stroke: the multicenter acute stroke trial—Europe study group. N Engl J Med 1996; 335:145–150.
2. Hacke W, Kaste M, Fieschi C, et al. Intravenous thrombolysis with recombinant tissue plasminogen activator for acute hemispheric stroke: the European Cooperative Acute Stroke Study. JAMA 1995; 274:1017–1025.
3. von Kummer R, Allen KL, Holle R, et al. Acute stroke: usefulness of early CT findings before thrombolytic therapy. Radiology 1997; 205:327–333.
4. Marchal G, Beaudouin V, Rioux P, et al. Prolonged persistence of substantial volumes of potentially viable brain tissue after stroke: a correlative PET-CT study with voxel-based data analysis. Stroke 1996; 27:599–606.
5. Furlan M, Marchal M, Viader F, Derlon JM, Baron JC. Spontaneous neurological recovery after stroke and the fate of the ischemic penumbra. Ann Neurol 1996; 40: 216–226.
6. Baird AE, Benfield A, Schlaug G, et al. Enlargement of human cerebral ischemic lesion volumes measured by diffusion-weighted magnetic resonance imaging. Ann Neurol 1997; 41:581–589.
7. Sorensen AG, Buonanno FS, Gonzalez RG, et al. Hyperacute stroke: evaluation with combined multisection diffusion-weighted and hemodynamically weighted echo-planar MR imaging. Radiology 1996; 199: 391–401.
8. Rosen BR, Belliveau JW, Aronen HJ, et al. Susceptibility contrast imaging of cerebral blood volume: human experience. Magn Reson Med 1991; 22:293–299.
9. Rosen B, Belliveau J, Buchbinder B, et al. Contrast agents and cerebral hemodynamics. Magn Reson Med 1991; 19:285–292.
10. Rosen B, Belliveau J, Vevea J, Brady T. Perfusion imaging with NMR contrast agents. Magn Reson Med 1990; 14:249–266.
11. Rosen BR, Aronen HJ, Kwong KK, Belliveau JW, Hamberg LM, Fordham JA. Advances in clinical neuroimaging: functional MR imaging techniques. RadioGraphics 1993; 13:889–896.
12. Østergaard L, Weisskoff R, Chesler D, Gyldensted C, Rosen B. High resolution measurement of cerebral blood flow using intravascular tracer bolus passages. I. Mathematical approach and statistical analysis. Magn Reson Med 1996; 36:715–725.
13. Østergaard L, Sorensen A, Kwong K, Weisskoff R, Gyldensted C, Rosen B. High resolution measurement of cerebral blood flow using intravascular tracer bolus passages. II. Experimental comparison and preliminary results. Magn Reson Med 1996; 36: 726–736.
14. Aronen H, Gazit I, Louis D, et al. Cerebral blood volume maps of gliomas: comparison with tumor grade and histologic findings. Radiology 1994; 191:41–51.
15. Boxerman J, Weisskoff R, Aronen H, Rosen B. Signal-to-noise and tissue blood volume maps from dynamic NMR imaging studies (abstr). In: Book of abstracts: Society of Magnetic Resonance in Medicine 1992. Berkeley, Calif: Society of Magnetic Resonance in Medicine, 1992; 1130.
16. Weisskoff R, Boxerman J, Sorensen A, Kulke S, Campbell T, Rosen B. Simultaneous blood volume and permeability mapping using a single Gd-based contrast injection (abstr). In: Proceedings of the Second Meeting of the Society of Magnetic Resonance. Berkeley, Calif: Society of Magnetic Resonance, 1994; 279.
17. Breiman R, Beck J, Korobkin M, et al. Volume determinations using computed tomography. AJR 1982; 138:329–333.
18. Warach S, Chien D, Li W, Ronthal M, Edelman RR. Fast magnetic resonance diffusion-weighted imaging of acute human stroke. Neurology 1992; 42:1717–1723.
19. Moseley ME, Mintorovitch J, Cohen Y, et al. Early detection of ischemic injury: comparison of spectroscopy, diffusion-, T2-, and magnetic susceptibility–weighted MRI in cats. Acta Neurochir Suppl (Wien) 1990; 51(suppl):207–209.
20. Welch K, Windham J, Knight R, et al. A model to predict the histopathology of human stroke using diffusion and T2-weighted magnetic resonance imaging. Stroke 1995; 26:1983–1989.
21. Lovblad KO, Baird AE, Schlaug G, et al. Ischemic lesion volumes in acute stroke by diffusion-weighted magnetic resonance imaging correlate with clinical outcome. Ann Neurol 1997; 42:164–170.
22. Rordorf G, Koroshetz W, Copen W, et al. Regional ischemia and ischemic injury in patients with acute middle cerebral artery stroke as defined by early diffusion-weighted and perfusion-weighted MRI. Stroke 1998; 29:939–943.
23. Weisskoff R, Chesler D, Boxerman J, Rosen B. Pitfalls in MR measurement of tissue blood flow with intravascular tracers: which mean transit time? Magn Reson Med 1993; 29:553–558.